Appl. Phys. A (2015) 119:667–672
DOI 10.1007/s00339-015-9011-9

Applied Physics A
Materials Science & Processing

Structural, electrical, and multiferroic properties of (Nd, Zn) co-doped $BiFeO_3$ thin films prepared by a chemical solution deposition method

Chinnambedu Murugesan Raghavan · Jin Won Kim · Sang Su Kim · Tae Kwon Song

Received: 10 December 2014 / Accepted: 20 January 2015 / Published online: 28 January 2015

Abstract The effects of Nd and Zn co-doping on the structural, electrical, and multiferroic properties of the $BiFeO_3$ thin film were investigated. Pure $BiFeO_3$ (BFO) and (Nd, Zn) co-doped $Bi_{0.9}Nd_{0.1}Fe_{0.975}Zn_{0.025}O_{3-\delta}$ (BNFZO) thin films were prepared on Pt(111)/Ti/SiO_2/Si(100) substrates by using a chemical solution deposition method. X-ray diffraction and Raman scattering analyses revealed the formation of polycrystalline distorted rhombohedral perovskite structures for both of the thin films. As compared to the pure BFO, a low leakage current density of 6.68×10^{-5} A/cm^2 (at 100 kV/cm), large remnant polarization ($2P_r$) of 60 μC/cm^2, and low coercive field ($2E_c$) of 773 kV/cm (at 1,000 kV/cm) were observed for the co-doped BNFZO thin film. Furthermore, the BNFZO thin film showed enhanced magnetization when compared to the BFO thin film. These results indicate that the randomly oriented BNFZO thin film would be a useful nontoxic alternative for lead-containing multiferroic applications.

1 Introduction

The perovskite-based bismuth ferrite $BiFeO_3$ (BFO) has attracted considerable interest because of its room-temperature multiferroic properties. In fact, it is the only room-temperature multiferroic material with high ferroelectric and magnetic transition temperatures, namely at 1,100 and 643 K, respectively [1]. BFO is known to have a rhombohedrally distorted perovskite structure with a *R3c* space group [2]. In the BFO crystal structure, a perovskite unit cell has a lattice parameter, a_{rh} of 3.965 Å with a rhombohedral angle of 89.4° at room temperature [3]. It was also described in the hexagonal crystal structure with lattice parameters, a_{hex} of 5.58 Å and c_{hex} of 13.90 Å. A large ferroelectric polarization has been reported along the pseudocubic $[111]_c$ axis, which is equal to the hexagonal $[001]_{hex}$ [3, 4]. In multiferroic BFO, the lone pair of electrons ($6s^2$) on the Bi ion acts as a source of ferroelectricity, whereas the magnetic properties originate from the partially filled *d*-orbital of the Fe^{3+} ion [5]. Its unusually large polarization and nontoxic nature afford BFO as a potential alternative for the highly toxic ferroelectric lead zirconium titanate [6].

In spite of its many advantages, BFO exhibits a low electrical resistivity due to a large leakage current, which leads to serious complications in practical ferroelectric devices [7]. The occurrence of a large electrical leakage in BFO has been attributed to the existence of oxygen vacancies and secondary phases, valence fluctuation of the Fe ions, rough surface features, and poor interfacial quality [8–12]. Doping of the Bi- and Fe-sites of the BFO with rare earth (*RE*) and transition metal (*TM*) ions has been strongly recommended as a way to reduce the leakage current density and to improve the multiferroic properties [13–18]. The use of *RE* ions as a dopant weakens the stereochemical activity of the Bi^{3+} $6s^2$ electron pairs, thereby resulting in the degradation of the ferroelectric polarization [19–21]. *TM* ions are known to reduce the concentration of oxygen vacancies by way of charge compensation [18]. Therefore, co-doping BFO with both *RE* and *TM* ions could be considered crucial for improving the ferroelectric properties of

C. M. Raghavan · J. W. Kim · S. S. Kim (✉)
Department of Physics, Changwon National University, Changwon, Gyeongnam 641-773, Republic of Korea
e-mail: sskim@changwon.ac.kr

T. K. Song
School of Nano and Advanced Materials Engineering, Changwon National University, Changwon, Gyeongnam 641-773, Republic of Korea

this material. A few reports describing the improvement of the electrical and ferroelectric properties of (Nd, *TM*) and (*RE*, Zn) double-ion modified BFO thin films have been published [22, 23]. However, to the best of our knowledge, (Nd, Zn) co-doped BFO thin films have not yet been studied before.

This study involved the preparation of both pure $BiFeO_3$ (BFO) and (Nd, Zn) co-doped $Bi_{0.9}Nd_{0.1}Fe_{0.975}Zn_{0.025}O_{3-\delta}$ (BNFZO) thin films on Pt(111)/Ti/SiO_2/Si(100) substrates by a chemical solution deposition method to investigate the structural, electrical, ferroelectric, and magnetic properties. The ionic radius of Nd^{3+} (1.27 Å) is smaller than that of Bi^{3+} (1.45 Å); therefore, the former is readily able to substitute into the Bi-site of the BFO. Furthermore, Bi-site substitution by Nd^{3+} ions could be expected to reduce the Bi volatility, suppress the formation of oxygen vacancies, and control the leakage current density [9], which is also reduced when the Fe-site is doped with Zn^{2+} [8, 9]. Therefore, the use of Nd and Zn ions to substitute the Bi- and Fe-sites of BFO could potentially modulate the electrical and ferroelectric properties of the material, because the advantageous effects of both of these sites can be utilized.

2 Experimental details

The raw materials used for the preparation of the precursor solutions were bismuth nitrate pentahydrate [$Bi(NO_3)_3$·$5H_2O$], iron nitrate nonahydrate [$Fe(NO_3)_3$·$9H_2O$], neodymium nitrate hexahydrate [$Nd(NO_3)_3$·$6H_2O$], zinc nitrate dihydrate [$Zn(NO_3)_2$·$2H_2O$], 2-methoxyethanol (2-MOE), and ethylene glycol (EG). A mixture of 2-MOE and EG was prepared by stirring for 30 min at 40 °C and was used as the solvent. Bismuth nitrate pentahydrate (5 mol% excess) was added to the above solvent and stirred for 30 min. To the above Bi-solution, acetic acid was added as a catalyst and stirred for 30 min. In the preparation process of the precursor solutions, acetic acid performs the role of a modifying ligand, and it also acts as an acid catalyst for the hydrolysis of the metal alkoxide [24]. In addition, it was also used to maintain the viscosity of the entire precursor solution to enable the thin film coating process to proceed in a uniform manner. Neodymium nitrate hexahydrate and zinc nitrate dihydrate were added to the Bi-solution with 30-min stirring intervals. Finally, iron nitrate nonahydrate was added to form the BNFZO solution. The resulting BNFZO solution was subjected to continuous stirring for 3 h to attain homogenization. A pure BFO precursor solution was also prepared as a reference by using the same method. The concentrations of the final solutions were adjusted to approximately 0.1 M.

A standard spin-coating method was used to prepare the BFO and the BNFZO thin films on Pt(111)/Ti/SiO_2/Si(100) substrates at a constant spinning rate of 3,000 rpm for 20 s. The wet films were prebaked at 360 °C for 10 min on a hot plate. The desired film thickness was obtained by repeating the coating and prebaking processes 12 times, after which both thin films were annealed at 550 °C for 30 min by a conventional thermal annealing process under a nitrogen atmosphere for crystallization. The Pt electrodes (with areas of 1.54×10^{-4} cm^2) were deposited on the top surfaces of the thin films by ion sputtering through a metal shadow mask to create a capacitor structure for electrical measurements.

An X-ray diffractometer (Rigaku, MiniFlex II) and a Raman spectroscope (Jasco, NRS-3100) were used to study the structures of the thin films. A field emission scanning electron microscope (Tescan, MIRA II LMH) was used to analyze the surface morphologies and the film thicknesses of the BFO and BNFZO thin films. The leakage current densities of the thin films were measured by an electrometer (Keithley, 6517A). The ferroelectric hysteresis loops of the thin films were measured at a frequency of 1.25 kHz with triangular pulses by a standardized ferroelectric test system (Radiant Technologies Inc., Precision LC). The room-temperature magnetic properties of the thin films were measured by using a physical property measurement system (Quantum Design Inc., PPMS-7).

3 Results and discussion

The X-ray diffraction (XRD) patterns of the BFO and the BNFZO thin films prepared on Pt(111)/Ti/SiO_2/Si(100) substrates are shown in Fig. 1. X-rays with $CuK_{\alpha 1}$ radiation

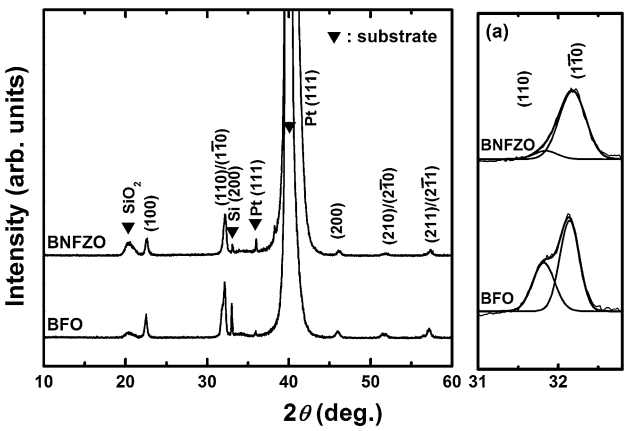

Fig. 1 XRD patterns of the BFO and the BNFZO thin films deposited on Pt(111)/Ti/SiO_2/Si(100) substrates. **a** Magnified XRD patterns with Lorentz fitted *curves* in the vicinity of $2\theta = 32.0^\circ$ corresponding to (110)/(1$\bar{1}$0) planes

($\lambda = 1.5418$ Å) were used. The XRD peaks observed for the BFO and the BNFZO thin films were indexed with reference to the polycrystalline distorted rhombohedral structure with a *R3c* space group [JCPDS No: 72-2035]. The XRD patterns contained no additional peaks corresponding to secondary or impurity phases, implying that the dopant concentrations did not reach the solubility limit of the BFO. Furthermore, there was no observable change in the lattice parameters for the BNFZO thin film, although the film was observed to display a small change in the diffraction patterns corresponding to the (110/1$\bar{1}$0) planes. As shown in Fig. 1a, the split peaks corresponding to the (110/1$\bar{1}$0) planes at 32° were clearly observed for the BFO thin film, whereas the corresponding peaks overlapped and appeared as a single peak on the diffraction pattern of the BNFZO thin film. However, a Gaussian fitting clearly indicated the presence of two peaks for the BNFZO thin film. This result indicates that the strain induced by the doping elements would increase the distortion induced in the perovskite layers without changing the original structure [25, 26]. Structural distortion of this nature has been reported to have a strong influence on the multiferroic properties [25].

The specific BFO sites, at which Nd and Zn ion substitution occurs, were examined by a Raman scattering spectral study. Figure 2 shows the Raman scattering spectra for the BFO and the co-doped BNFZO thin films measured at room temperature. The exact peak positions were assigned by fitting the measured spectra and decomposing the fitted curves into their individual Lorentz components. According to group theoretical studies, 13 ($4A_1 + 9E$) fundamental active modes are predicted for rhombohedrally distorted perovskites with a *R3*c space group [1]; hence, the active modes that were observed in the present investigation are in good agreement with the rhombohedrally distorted perovskite structure. The longitudinal optical (*LO*) and transverse optical (*TO*) modes were indexed for the BFO and the BNFZO thin films with reference to the literature [27]. All of the observed Raman active modes for the thin films are given in Table 1. For the BFO thin film, the low-frequency Raman modes observed at 137, 168, and 216 cm^{-1} were assigned as $A_1(1LO)$, $A_1(2LO)$, and $A_1(3LO)$, with the high-frequency modes at 257, 279, 309, 341, 363, 467, and 610 cm^{-1} assigned as *E*(*TO*), *E*(*TO*), E(*TO*), *E*(*TO*), *E*(*TO*), *E*(*TO*), and *E*(*TO*), respectively. In the case of the BNFZO thin film, the $A_1(1LO)$, $A_1(2LO)$, and $A_1(3LO)$ modes were observed at 142, 167, and 219 cm^{-1}, respectively, whereas the Raman modes at 274, 320, 370, 430, and 603 cm^{-1} were assigned to the *E*(*TO*), *E*(*TO*), *E*(*TO*), *E*(*TO*), and *E*(*TO*) modes, respectively. The A_1 active modes observed in the low-frequency region have been attributed to the Bi–O vibration and the high-frequency *E* modes to the Fe–O vibration [28]. As shown in Fig. 2, for the BNFZO thin film, the peak intensity was observed to change, and the peaks were observed to broaden at low frequencies, both of which can be attributed to the doping of the Bi-site of the BFO with Nd ions [20]. Nd ion doping of the Bi-site of the BFO leads to a dispersion of Bi–O bonding, which in turn affects the active modes in the low-frequency region. The formation of an intense peak at 603 cm^{-1} for the BNFZO thin film was attributed to structural changes in the [FeO_6] octahedra and indicates the combined doping effects of the Nd and Zn ions [29]. The small shifts of the peaks in the high-frequency region of the spectrum of the co-doped BNFZO thin film might be related to the doping of Zn ion into the Fe-site [29].

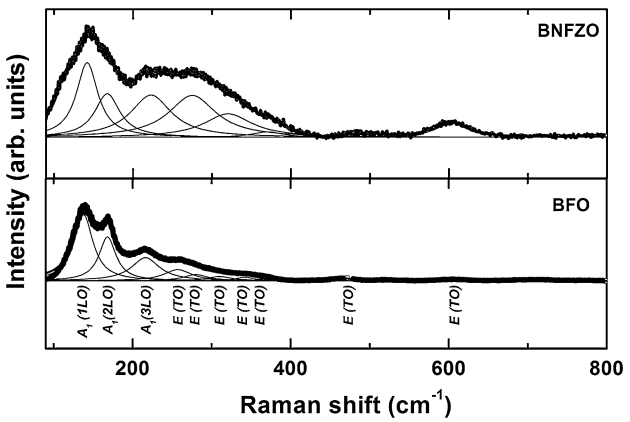

Fig. 2 Raman scattering spectra with fitted curves (*thick solid lines*) and the decomposed active modes (*thin solid lines*) of the BFO and the BNFZO thin films measured at room temperature

The surface morphologies of the BFO and the BNZO thin films are shown in Fig. 3 together with their cross-sectional micrographs. The doping of Nd and Zn ions into the Bi- and Fe-sites of BFO influences nucleation and leads to significant change in the microstructural features. The SEM image shows the surface morphology of the BFO thin film to be rough with the formation of micropores, whereas the BNFZO thin film exhibited a smooth surface in comparison. The Nd–O bond energy (703 kJ/mol) is higher than that of the Bi–O bond (337 kJ/mol), which increases the amount of heat that is released during film growth, in turn stabilizing the structure to maintain the smooth surface [30]. The thicknesses of the BFO and the BNFZO thin films were approximately 300 and 350 nm, respectively, as determined from the cross-sectional SEM images.

Figure 4 shows the plots of the leakage current densities (*J*) as a function of the applied electric fields (*E*) for both the BFO and the BNFZO thin films, for which *J* values of 2.58×10^{-3} and 6.68×10^{-5} A/cm^2 were measured at an applied electric field of 100 kV/cm, respectively. Thus, the *J* value of the BNFZO thin film was found to be two orders

Table 1 Comparison of the Raman frequencies observed for the BFO and the BNFZO thin films

Samples	A_1 (*1LO*)	A_1 (*2LO*)	A_1 (*3LO*)	*E* (*TO*)						
BFO	137	168	216	257	279	309	341	363	467	610
BNFZO	142	167	219	–	274	320	–	370	430	603

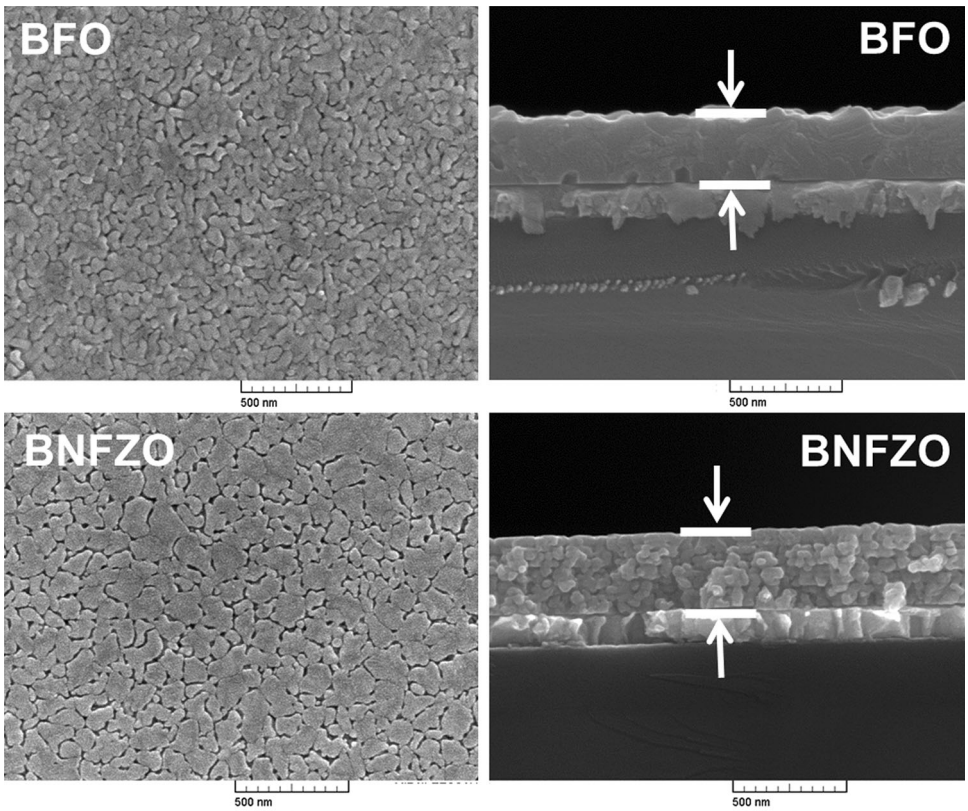

Fig. 3 SEM images of the surface morphologies and cross-sectional views of the BFO and the BNFZO thin films

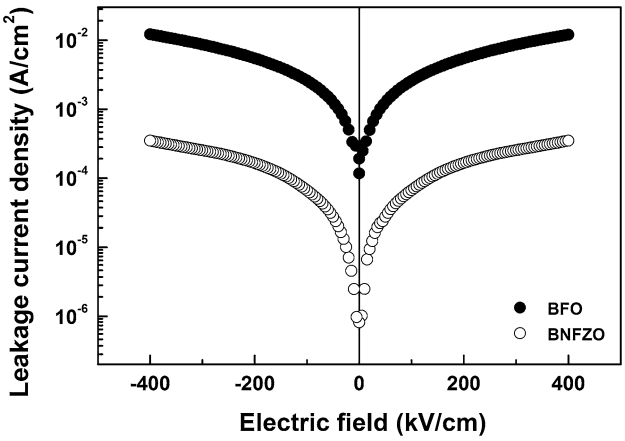

Fig. 4 Leakage current densities of the BFO and the BNFZO thin films

of magnitude lower than that of the BFO thin film. The large leakage current density of the BFO thin film is attributed to the presence of a large number of oxygen vacancies [8], partially caused by the ease with which the Bi ion is able to evaporate from BFO during the preparation of the thin film [9]. The lower leakage current density of the BNFZO thin film can be related to a decrease in the concentration of oxygen vacancies of which the energy levels are very close to those of the conduction band in the perovskite BFO [31]. Therefore, the formation of oxygen vacancies would enable the material to readily conduct electric current by promoting an electric cloud with respect to the applied electric field [32]. In addition, the Nd–O bond (703 kJ/mol) is stronger than the Bi–O (337 kJ/mol) bond; hence, Nd substitution controls the Bi evaporation and stabilizes the perovskite structure [9, 17, 18]. At the

same moment, the doping of divalent Zn ions into the Fe-sites of the BFO was reported to enable the formation of a defect complex between the Zn^{2+} ion and oxygen vacancies as represented by $[(Zn^{2+}_{Fe^{3+}})' - (V^{\cdot\cdot}_{O^{2-}})]$ [32]. Breaking this defect complex to provide free charge carriers to enable conduction requires a large electric field [32]. The formation of grain clusters with a smooth surface might also play a role in reducing the leakage current of the co-doped BNFZO thin film.

The multiferroic properties of the BFO and the BNFZO thin films were evaluated by investigating the ferroelectric and ferromagnetic properties at room temperature. Figure 5 shows the ferroelectric polarization–electric field (P–E) hysteresis loops of the BFO and the BDFZO thin films. An analysis of the hysteresis loops revealed a small remnant polarization ($2P_r$) of 36 μC/cm^2 and a large coercive field ($2E_c$) of 1,365 kV/cm at an applied electric field of 1,060 kV/cm for the BFO thin film. The $2P_r$ and the $2E_c$ values of the BNFZO thin film were 60 μC/cm^2 and 773 kV/cm at an applied electric field of 1,000 kV/cm, respectively. The improved ferroelectric properties of the BNFZO thin films are attributed to the combined effect of co-doping with Nd and Zn ions. The use of ions with small ionic radii and a large electronegativity as dopants leads to a more pronounced off-center displacement in the BFO. The ionic radius of Nd^{3+} (1.27 Å) is smaller than that of Bi^{3+} (1.45 Å). Therefore, it can easily substitute into the Bi-site of the BFO. In addition, as the electronegativity difference between Nd and O is larger than that between Bi and O, the doping of Nd ions into the Bi-site of the BFO might lead to a more pronounced off-center distortion, which would in turn enhance the ferroelectric properties [33]. However, the substitution of Nd^{3+} ion into the Bi-site has been reported to weaken the stereochemical activity of the lone electron pair of Bi and the Bi–O covalent bonds, which would in turn degrade the ferroelectricity [21]. In this study, the (Nd, Zn) co-doped BNFZO thin film exhibited enhanced ferroelectric properties compared to BFO doped with Nd alone [34]. Hence, the role of the Zn ion appears to be very important for the improvement of the ferroelectric properties. The divalent Zn^{2+} ions facilitate the formation of the defect complex$[(Zn^{2+}_{Fe^{3+}})' - (V^{\cdot\cdot}_{O^{2-}})]$, which may also influence the ferroelectric polarization [32]. Furthermore, the ability of the Nd and Zn ions to stabilize the formation of the perovskite phase and to reduce the number of oxygen vacancies in the BNFZO thin film favors a large polarization and a low coercive field.

The magnetic properties were studied by measuring the magnetization (M) versus the magnetic field (H) hysteresis loops of the BFO and the BNFZO thin films at room temperature, and are shown in Fig. 6, in which it can be seen that both of the thin films exhibited weak ferromagnetism with well-saturated M–H hysteresis loops. The measured remnant magnetization ($2M_r$) and coercive magnetic field ($2H_c$) values of the BFO and the BNFZO thin films were 0.028 emu/cm^3 and 0.29 kOe, and 0.037

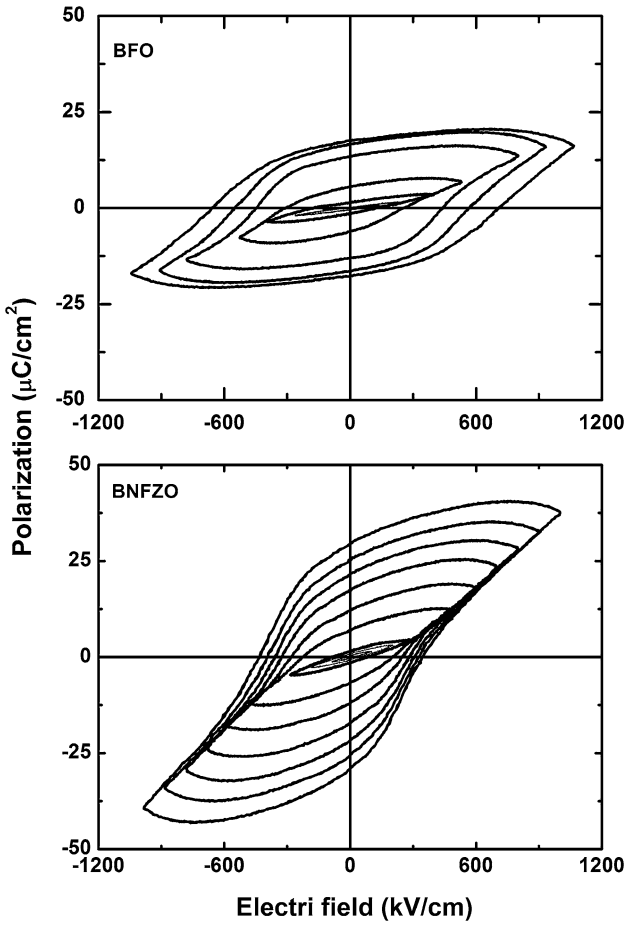

Fig. 5 Ferroelectric P–E hysteresis loops of the BFO and the BNFZO thin films

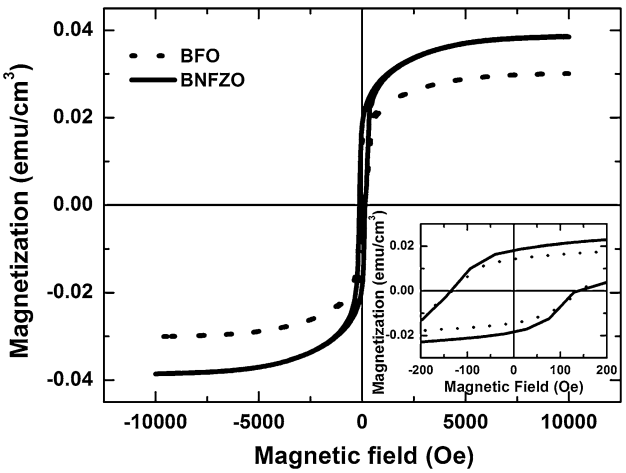

Fig. 6 Magnetic M–H hysteresis loops of the BFO and the BNFZO thin films

emu/cm^3 and 0.27 kOe at an applied magnetic field of 10 kOe, respectively. The magnetic structure of BFO was demonstrated with respect to G-type antiferromagnetic ordering, while it also exhibits a weak ferromagnetic ordering due to canting of the electron spin in the unit cell [35]. The magnetic interaction between the Fe ions can also lead to spontaneous magnetization in the BFO thin film [35]. This phenomenon might also be responsible for the weak ferromagnetism that was observed for both of the BFO and the BNFZO thin films. However, compared to the BFO thin film, the BNFZO thin film exhibited enhanced magnetization. This could be attributed to the structural distortion caused by the Nd^{3+} and Zn^{2+} ions, which would result in a tilting of the octahedra to release the locked magnetization from the spiral spin structure of the BFO [35].

4 Conclusions

The effects of (Nd, Zn) co-doping on the structural, electrical, and multiferroic properties of the BFO thin films prepared on Pt(111)/Ti/SiO_2/Si(100) substrates via chemical solution deposition were investigated. Distorted rhombohedral perovskite structures for the BFO and the BNFZO thin films were confirmed by XRD and Raman scattering analyses. Compared to the pure BFO, the co-doped BNFZO thin film showed a large remnant polarization, reduced leakage current density, and low coercive field. The enhanced electrical properties of the BNFZO thin film could be explained by the combined effect of the reduced concentration of oxygen vacancies and changes in the microstructural features. The enhanced multiferroic properties of the BNFZO thin film was related to structural distortion.

Acknowledgments This work was supported by the Priority Research Centers Program through the National Research Foundation of Korea (NRF) Funded by the Ministry of Education, Science and Technology (2010-0029634).

References

1. M.K. Singh, H.M. Jang, S. Ryu, M.H. Jo, Appl. Phys. Lett. **88**, 042907 (2006)
2. J.M. Moreau, C. Michel, R. Gerson, W.J. James, J. Phys. Chem. Solids **32**, 1315 (1971)
3. G. Catalan, J.F. Scott, Adv. Mater. **21**, 2463 (2009)
4. V.V. Lazenka, G. Zhang, J. Vanacken, I.I. Makoed, A.F. Ravinski, V.V. Moshchalkov, J. Phys. D Appl. Phys. **45**, 125002 (2012)
5. N.A. Hill, J. Phys. Chem. B **104**, 6694 (2000)
6. Y.H. Chu, Q. Zhan, L.W. Martin, M.P. Cruz, P.L. Yang, G.W. Pabst, F. Zavaliche, S.Y. Yang, J.X. Zhang, L.Q. Chen, D.G. Schlom, I.N. Lin, T.B. Wu, R. Ramesh, Adv. Mater. **18**, 2307 (2006)
7. S.K. Singh, K. Maruyama, H. Ishiwara, Appl. Phys. Lett. **91**, 112913 (2007)
8. X.D. Qi, J. Dho, R. Tomov, M.G. Blamire, J.L.M. Driscoll, Appl. Phys. Lett. **86**, 062903 (2005)
9. Z. Hu, M. Li, Y. Yu, J. Liu, L. Pei, J. Wang, X. Liu, B. Yu, X. Zhao, Solid State Commun. **150**, 1088 (2010)
10. G.L. Yuan, S.W. Or, H.L.W. Chan, Z.G. Liu, J. Appl. Phys. **101**, 024106 (2007)
11. H. Yang, Y.Q. Wang, H. Wang, Q.X. Jia, Appl. Phys. Lett. **96**, 012909 (2010)
12. J.F. Scott, C.A. Araujo, B.M. Melnick, L.D. McMillan, R. Zuleeg, J. Appl. Phys. **70**, 382 (1991)
13. I. Coondoo, N. Panwar, I. Bdikin, V.S. Puli, R.S. Katiyar, A.L. Kholkin, J. Phys. D Appl. Phys. **45**, 055302 (2012)
14. Z. Cheng, X. Wang, S. Dou, H. Kimura, K. Ozawa, Phys. Rev. B **77**, 092101 (2008)
15. B. Yu, M. Li, J. Liu, D. Guo, L. Pei, X. Zhao, J. Phys. D Appl. Phys. **41**, 065003 (2008)
16. J. Wu, J. Wang, J. Am. Ceram. Soc. **93**, 2795 (2010)
17. G.D. Hu, X. Cheng, W.B. Wu, C.H. Yang, Appl. Phys. Lett. **91**, 232909 (2007)
18. C.M. Raghavan, D. Do, J.W. Kim, W.-J. Kim, S.S. Kim, J. Am. Ceram. Soc. **95**, 1933 (2012)
19. S. Zhang, L. Wang, Y. Chen, D. Wang, Y. Yao, Y. Ma, J. Appl. Phys. **111**, 074105 (2012)
20. G.L. Yuan, S.W. Or, H.L.W. Chan, J. Appl. Phys. **101**, 064101 (2007)
21. I.O. Troyanchuk, M.V. Bushinsky, D.V. Karpinsky, O.S. Mantytskaya, V.V. Fedotova, O.I. Prochnenko, Phys. Stat. Sol. B **246**, 1901 (2009)
22. J. Wu, J. Wang, Electrochem. Solid-State Lett. **13**(12), G105 (2010)
23. C.M. Raghavan, J.W. Kim, S.S. Kim, Ceram. Inter. **39**, 3563 (2013)
24. R.W. Schwartz, Chem. Mater. **9**, 2325 (1997)
25. X. Zhang, Y. Sui, X. Wang, Y. Wang, Z. Wang, J. Alloys Compd. **507**, 157 (2010)
26. F. Yan, M.O. Lai, L. Lu, T.J. Zhu, J. Phys. Chem. C **114**, 6994 (2010)
27. J. Wu, J. Wang, Act. Mater. **58**, 1688 (2010)
28. P. Hermet, M. Goffinet, J. Kreisel, Ph Ghosez, Phys. Rev. B **75**, 220102 (2007)
29. G. Kartopu, A. Lahmar, S. Habouti, C.-L. Solterbeck, B. Elouadi, M. Es-Souni, Appl. Phys. Lett. **92**, 151910 (2008)
30. V.V. Lazenka, M. Lorenz, H. Modarresi, K. Brachwitz, P. Schwinkendorf, T. Böntgen, J. Vanacken, M. Ziese, M. Grundmann, V.V. Moshchalkov, J. Phys. D Appl. Phys. **46**, 175006 (2013)
31. S.J. Clark, J. Robertson, Appl. Phys. Lett. **94**, 022902 (2009)
32. G.D. Hu, S.H. Fan, C.H. Yang, W.B. Wu, Appl. Phys. Lett. **92**, 192905 (2008)
33. F. Yan, M.O. Lai, L. Lu, J. Phys. D Appl. Phys. **45**, 325001 (2012)
34. A. Kumar, D. Varshney, Ceram. Inter. **38**, 3935 (2012)
35. J. Wei, R. Haumont, R. Jarrier, P. Berhtet, B. Dkhil, Appl. Phys. Lett. **96**, 102509 (2010)